Design, Fabrication, and Measurements of an RF-MEMS-Based Self-Similar Reconfigurable Antenna

Dimitrios E. Anagnostou, *Member, IEEE*, Guizhen Zheng, *Member, IEEE*, Michael T. Chryssomallis, *Senior Member, IEEE*, James C. Lyke, George E. Ponchak, *Senior Member, IEEE*, John Papapolymerou, *Senior Member, IEEE*, and Christos G. Christodoulou, *Fellow, IEEE*

***Abstract*—Reconfigurability in an antenna system is a desired characteristic that has been the focus of much research in recent years. In this work, ohmic contact cantilever RF-MEMS switches are integrated with self-similar planar antennas to provide a reconfigurable antenna system that radiates similar patterns over a wide range of frequencies. The different issues encountered during the integration of the MEMS switches and the overall system design procedure are described herein. The final model radiates at three widely separated frequencies with very similar radiation patterns. The proposed concept can be extended to reconfigurable linear antenna arrays or to more complex antenna structures with large improvements in antenna performance.**

***Index Terms*—Fractal, reconfigurable antennas, RF-MEMS, self-similar, Sierpinski, silicon.**

I. Introduction

RECONFIGURABLE RF-MEMS antenna systems were first introduced in 1998 by E. R. Brown [1] and since then have been studied by several research groups. An emphasis has been given in reconfigurable aperture (recap) and microstrip antenna structures, in order to achieve multiple octave tuneability [2]–[5]. However, the integration of RF-MEMS with the antenna has not been fully demonstrated. Furthermore, in the majority of publications, ideal models for the switches have been used while the effect of the bias lines on the antenna performance has been largely neglected.

The radiation patterns of an antenna are inherently related to the distributions of the currents on its surface. Predetermination of these current paths, allows one to define the antenna's radiation patterns at its various frequencies of operation. The feature of self-similarity of a fractal antenna can provide a basis for the design of multiple-frequency antennas. These antennas have the advantage that they radiate similar patterns in a variety of frequency bands. The major predecessor is the widely studied Sierpinski gasket [6], [7]. In an ideal case, the Sierpinski gasket is described by an infinite number of iterations resulting in a very complex antenna structure with an infinite number of frequency bands. In reality though, technological limitations reduce the number of iterations for such a structure to a finite one, usually less than 6 (pre-fractal). Moreover, for the purposes of this paper, only 1 iteration was found necessary to obtain the desired reconfigurability but more complex designs will be examined in the future.

So far, the Sierpinski gasket has been modified in several ways to give desirable frequency spacing [8]–[10]. In [11], low-pass filters were applied between the triangle interconnections to suppress any sidelobes that may exist after the 1st resonance. The great majority of research regarding Sierpinski gasket antennas has been done for a structure etched on thin dielectric materials with low relative permittivity, thus approximating the free-space environment.

In a previous work, preliminary results on a similar antenna fabricated on silicon were reported [12]. The current paper examines several issues that appear before, during, and after the antenna integration. These are with respect to its design, feed, and performance as well as with the structure and the biasing network of the used RF-MEMS switches. The main idea is to demonstrate the function of a new type of RF-MEMS reconfigurable multiband antenna based on a self-similar design. Such an antenna enhances the performance of a conventional Sierpinski gasket by adding to it one frequency band. An analytical procedure used to design the antenna is also introduced. Finally, simulated and measured results demonstrating the antenna's functionality for the different states of its RF-MEMS switches are presented and discussed.

II. RF-MEMS Switches and Antenna Design

MEMS switches have shown good RF characteristics and can be used at both low and high frequency applications [13]. The switches used herein exhibited better performance compared to PIN diodes and FET transistors, up to approximately 40 GHz, regarding insertion loss, isolation, power consumption

Manuscript received February 16, 2005; revised June 30, 2005. This work was supported in part by the Georgia Electronic Design Center, by NSF under Grant ECS#0218732 and by Mission Research Corporation under Contract SC-0244-0008, UNM-1).

D. E. Anagnostou was with the University of New Mexico, Albuquerque, NM 87106 USA. He is currently with the Georgia Institute of Technology, Atlanta, GA 30308 USA (e-mail: danagn@ieee.org).

G. Zheng was with the Georgia Institute of Technology, Atlanta, GA 30308 USA. She is currently with Intel Corporation, Phoenix, AZ 85044 USA.

M. T. Chryssomallis is with the Democritus University of Thrace, Polytechnic School of Xanthi, Xanthi, 67100, Greece.

J. C. Lyke is with the Air Force Research Laboratory, Kirtland AFB, Albuquerque, NM 87117 USA.

G. E. Ponchak is with the NASA Glenn Research Center, Cleveland, OH 44135 USA.

J. Papapolymerou is with the Georgia Institute of Technology, Atlanta, GA 30308 USA.

C. G. Christodoulou is with the University of New Mexico, Albuquerque, NM 87106 USA.

Digital Object Identifier 10.1109/TAP.2005.863399

0018-926X/$20.00 © 2006 IEEE

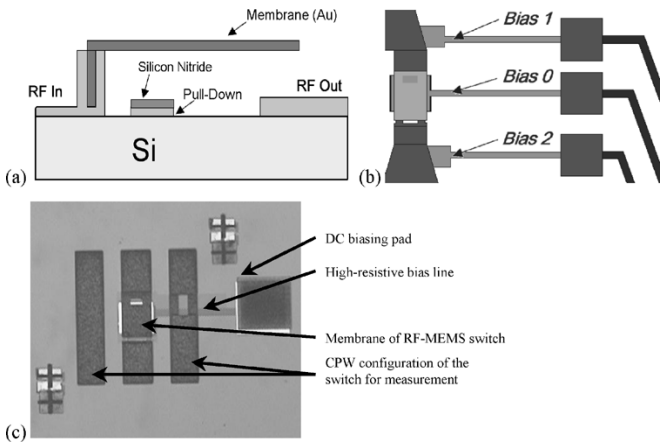

Fig. 1. (a) Schematic cross-section of the switch model. (b) Top view of the switch model illustrating the bias lines. (c) Photograph of the fabricated switch.

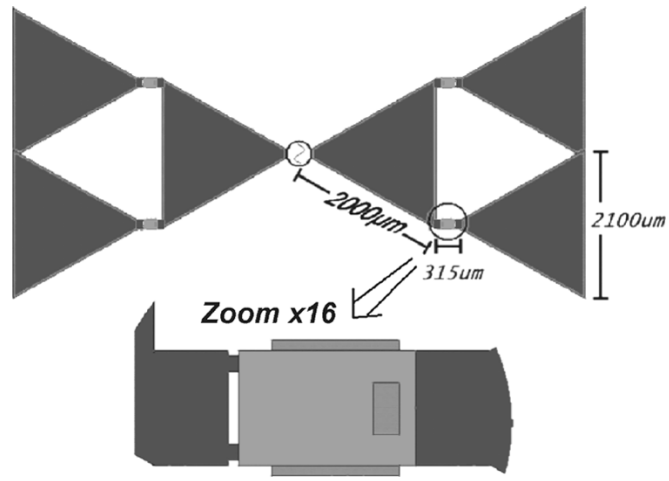

Fig. 2. Initial antenna design and RF-MEMS switch connections.

and linearity. They have also proven to be reliable if packaged appropriately. They are based on an electrostatically actuated suspension membrane or cantilever, and the biasing voltage is a function of the area of the cantilever that is directly above the biasing electrode, the distance of the beam from the electrode when the cantilever is up, the relative permittivity of the dielectric material between the beam and the electrode, and the flexibility and thickness of the membrane material. Switching times of 5–30 μs have been achieved. The biasing voltage determines also the minimum distance between the biasing lines according to the breakdown voltage of the substrate material. The bias lines were placed at a distance that withstands more than 5 times higher voltage than the one used. Side and top view illustrations of the switch are shown in Fig. 1(a) and (b). A photo of the fabricated model is shown in Fig. 1(c).

The first reconfigurable antenna studied herein is a planar 1-iteration Sierpinski gasket with a 60° bow-angle and 3800 μm height on each arm. To obtain the desirable reconfigurability, the antenna's adjacent triangular patches are connected with 4 series cantilever ohmic contact RF-MEMS switches. The introduction of these electrostatic actuators permits the physical connection/disconnection of sections of the antenna's conductive parts relative to each other. The new reconfigurable antenna may contain both similar and dissimilar radiating (or receiving) elements. Using these switches, a bowtie mode of operation (all switches OFF) and a MEMS-enabled (or fractal) mode of operation (all switches ON) can be obtained. Since the 'fractal' mode's active structure consists of one iteration, we anticipate two widely-spaced resonant frequencies. Two more nonsymmetric configurations may also be obtained by setting one switch ON and one OFF on each arm. The result is a total of 4 different paths for the currents to flow and hence 4 possible antenna configurations. As previously mentioned, the self-similarity between the 2 major modes (bowtie and fractal) results in similar radiation patterns. The two nonsymmetric modes exhibited simulated patterns similar to the planar dipole as well but were not measured. The initial antenna dimensions and the placement of the switches are shown in Fig. 2. Proper connection and function of the electrostatic actuators imposes many structural restrictions on the antenna's materials and especially on its substrate layers as described in the next section.

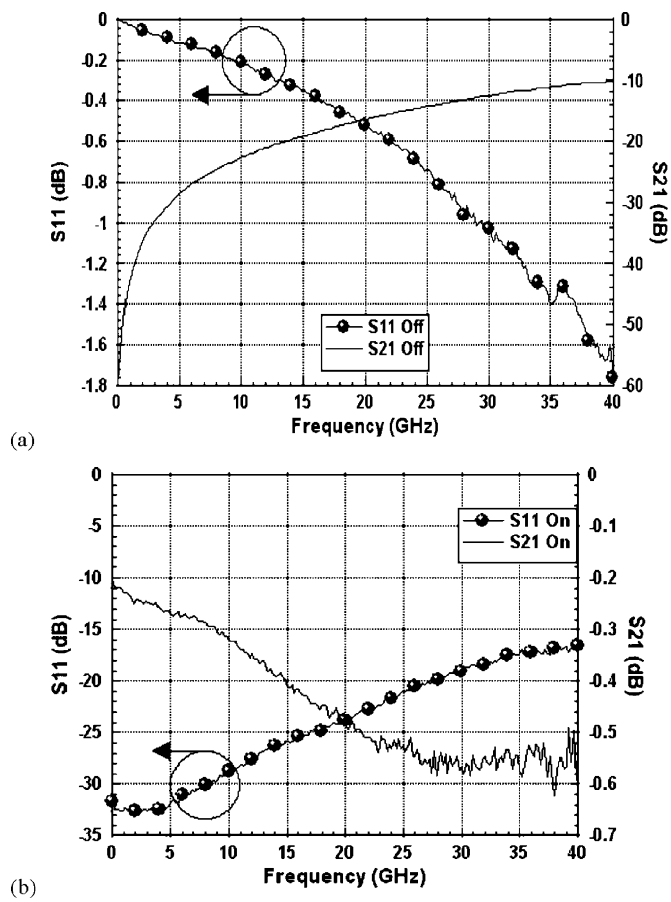

Fig. 3. (a) Measured S-parameters of the switch at the OFF state. (b) Measured S-parameters of the switch at the ON state.

III. Integration of RF-MEMS Switches With the Antenna

The cantilever ohmic contact switch is fabricated on a 400 μm high-resistivity ($\rho > 10$ KΩ-sq) silicon wafer and has a flexible membrane made of gold (*Au*) that is suspended 2 μm above the bottom electrode, as shown in the schematic of Fig. 1(a). This places the need for the antenna to be printed on the same substrate material in order to connect properly to the switches. It is also preferable that the antenna is made of the same material as

the metal layer of the switch. The antenna is fabricated monolithically with the MEMS switches on the same substrate. Electrostatic biasing occurs on demand by applying a dc voltage of approximately 40 Volts between the probe pad that is connected to the pull-down electrode and the membrane. The switch was fabricated and measured at the Georgia Institute of Technology and its performance is shown in Fig. 3(a) and (b). The insertion loss when the switch is ON is around 0.2 dB at 15 GHz, while the additional 0.2 dB measured loss is due to the transmission line used in the measurement. When the switch is OFF, isolation is around 18 dB at 15 GHz. The overall switch performance reveals that it can be used in antenna applications for frequencies up to 40 GHz.

The accuracy of the applied potential difference is ensured by two more biasing lines which provide the dc ground to the switch. The dc biasing pads for each switch are placed 2500 μm away from the furthest conductive part of the antenna, to minimize the deformation of the radiation pattern caused by the metallic surface of the probe heads. The connections of the bias lines on a switch appear in Fig. 1(b), where *Bias 1* and *Bias 2* refer to the ground, and *Bias 0* is where the dc voltage is applied. Since the bias lines are conductive, one may think that any metal such as copper (*Cu*) or *Au* can be used. However, metallic bias lines completely alter the antenna's behavior as shown next.

The bias lines pass close to the antenna and parallel to its edges. This way, if any energy is radiated from them, it will interfere constructively with the antenna's radiation pattern. At the points where the bias lines connect to the switches, the currents surface density increases and currents begin to flow on the lines' conducting paths causing undesired resonances. For example, even though the antenna is designed to resonate at 14 GHz when the switches are OFF, a bias line (*bias 2*) introduces a resonance at 7 GHz due to its length being almost twice than the antenna's maximum active edge length. These bias lines also alter the radiation pattern at 14 GHz, which is the primary desired frequency. The above are illustrated in Fig. 4, where simulated results of the average current surface density on the lines and switch area at 7 GHz and the antenna's frequency response with all switches OFF are shown. To avoid the effects of the metallic bias lines, one must use high-resistive materials for their construction.

The high – resistive material used in this work is aluminum-deposited zinc oxide (AZO) and it was deposited with combustion chemical vapor deposition. Sheet resistance is around $R_{\mathrm{s}} = 10\ \mathrm{K}\Omega/\mathrm{sq}$ and each resistive line was designed to be at least 20 squares long, providing a total measured dc resistance of more than 200 $\mathrm{K}\Omega$ that causes RF currents to attenuate quickly. Deformation of the antenna's radiation patterns is minimal and the slight extension of the currents' path causes only a slight shift of the resonant frequencies. The antenna is designed to have three bands: 14 GHz (switches OFF), 8 GHz and 23 GHz (switches ON). The maximum effect of the bias lines on the antenna's performance occurs at the higher frequencies, and simulated currents at 23 GHz are shown in Fig. 5(a). The biasing network is shown in Fig. 5(b) for visualization purposes. A comparison of the antenna's frequency performance with and without the bias network is shown in Fig. 5(c) and (d). The bias lines conclude in dc pads, of 150 and 400 pitch. The dc bias is applied from the top and bottom of the antenna, while the RF from the side. This leaves open the capability to extend the RF

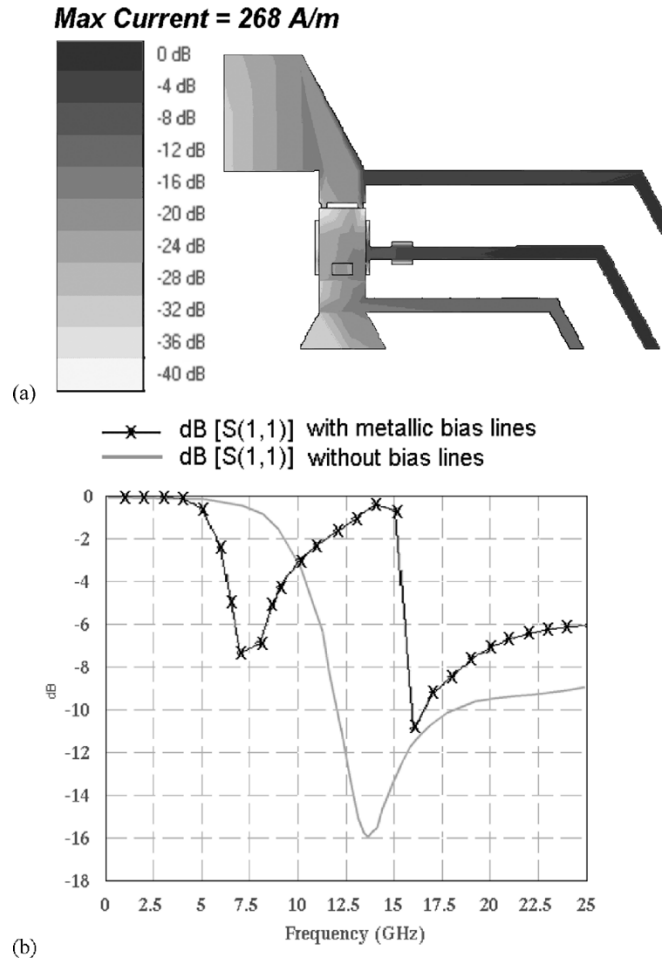

Fig. 4. (a) Simulated current distribution at 7 GHz. (b) Simulated S_{11} of the antenna with metallic bias lines.

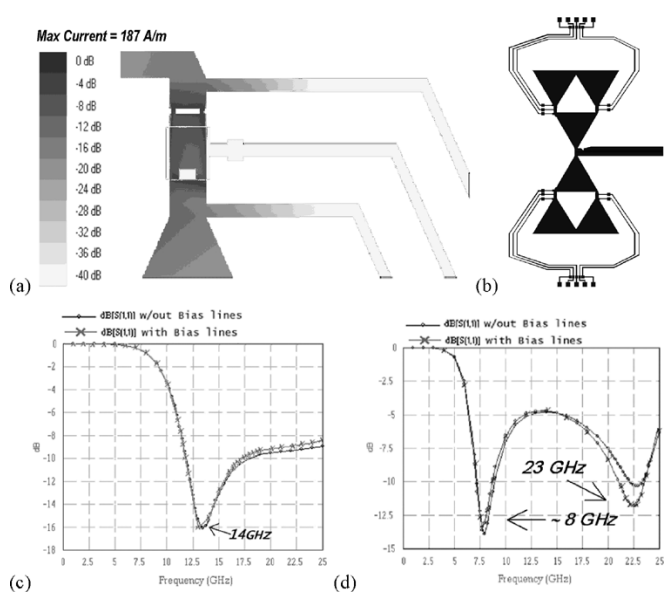

Fig. 5. (a) Simulated currents on the high-resistive bias lines at 23 GHz. (b) Entire antenna layout for visualization of the bias network. (c) Comparison of S_{11} with and without high-resistive bias lines when switches are OFF and (d) when switches are ON.

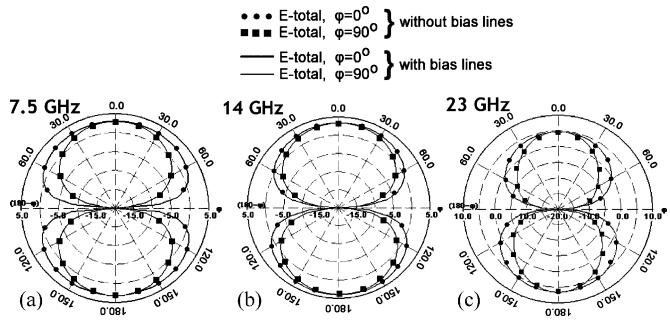

Fig. 6. (a)-(c) Superimposed radiation patterns with and without bias network at the antenna's resonant frequencies. Minor differences result in almost coinciding patterns.

feed and connect more planar antennas (similar or dissimilar), thus creating a reconfigurable, multiple-frequency linear array.

As mentioned before, the effect of the bias network on the antenna's radiation patterns should be minimal at any frequency of operation. In Fig. 6(a)–(c), the radiation patterns for each resonance, with and without bias lines are superimposed. It can be noticed that in all three modes the patterns almost coincide implying that the lines' effect is minimal.

IV. Antenna Feed Transition

To feed this type of planar antenna, a balanced type of feed that will set the voltage on its terminals to a 180° phase-difference is required. A coplanar waveguide (CPW) to coplanar stripline (CPS) transition was designed to feed the antenna in such a balanced way. The transition maintains a 50 Ω characteristic impedance and ends in pads with 150 μm pitch. It is fabricated on the same substrate as the antenna and enables the measurement of the antenna's performance using the available RF probes. The design and performance description of the transition are out of the scope of this paper and therefore omitted. The interested reader may refer to [14], [15] for the transition's design and performance. It is worth-mentioning though that the CPS line is complementary to CPW line and that the design equations used for the CPS and CPW parts can be found in [16] and [17], respectively.

V. Improved Antenna Design

Even though this first antenna design has good characteristics, its performance (shown in Fig. 5) shows relatively shallow resonances, with respect to a return loss $S_{11} = -10\,\mathrm{dB}$, that can be improved. Also, the fabrication of the reconfigurable antenna is a complicated multi-layered process and a successful integration requires careful preparation for every step in order not to deteriorate the antenna's performance. Among those steps, the most critical processes can be summarized in: 1) dc bias line patterning, 2) deposition and the patterning of the thin layer of dielectric material for the MEMS switches, and 3) fabrication and release process of the switch membrane.

1) The dc bias lines consist of two different materials, the highly resistive (AZO) and the conductive thin layer of *Au* in connection with the dc probe pads. They are done with chemical etching and lift off process respectively, and they need to be well controlled to provide a high resistive dc line as well as a good contact with the dc probe pad. If the resistivity of the dc line is not high enough, there will be RF energy leakage through those lines; additionally, if the dc lines are not in good contact with the dc probe pads, or if there is a poor contact between the AZO and the thin layer of *Au*, the dc actuation voltage won't be supplied to the MEMS switches effectively.
2) The second category is the deposition and the patterning of the thin layer of the silicon nitride (Si_3N_4) dielectric material. The thickness, smoothness and uniformity have to be well controlled to provide a good isolation layer between the membrane and the bottom electrode of the MEMS switches. Inaccuracies during this step may result in either low break down voltage or in a severe dielectric charge problem of the switches.
3) The third and most important category is the membrane fabrication and release process. Here, a) the deposition of the seed layer of the membrane must be well controlled and monitored in order not to crush the sacrificial layer underneath it, b) the plating speed and temperature should be controlled in order to minimize the membrane deformation due to the different metal stress, and c) the drying process should prevent the MEMS from stiction problems.

Inaccuracies during the first step a) mentioned above can lead to current leakage, thus degrade the antenna performance. Inaccuracies in the second and third steps b) and c) can lead to the failure of the proper function of the MEMS switches and thus to a system failure.

All the above problems can be avoided if the process is well controlled. On the other hand, and in addition to the above, the bulky RF and dc probes will inevitably interfere with the antenna's radiation patterns and input impedance. Even though the probes have been placed relatively far from the system's radiating area, simulations did not take into account their effects. The reason for this was their large volume, compared with the wavelengths at the frequencies of operation, that would result in large computer memory requirements. The distance of the probes from the antenna was selected to be of several wavelengths, in order to minimize these interference phenomena.

As already mentioned, the antenna should not only be better matched at each configuration but also maintain the dipole-like form of its radiation patterns. The bowtie mode has a bandwidth of 6 GHz (full Ku band) from 12 to 18 GHz, which may not all necessarily be required. An analytical step-by-step procedure to address this issue and so to improve antenna matching at the expense of its available bandwidth is investigated. Self-similarity is maintained while only the antenna's bow-angle is varied for all configurations, and the one that yields the optimum antenna performance is selected for the final design. A schematic of the procedure's stages is shown in Fig. 7.

A. Bowtie in Free Space

First we consider a bowtie antenna in free space. Its input impedance in free-space was studied by Booker in [18]. His relations do not hold accurately for our structure, as the near-field interactions with the substrate cause a perturbation of the antenna's input impedance. This impedance is scaled by a factor

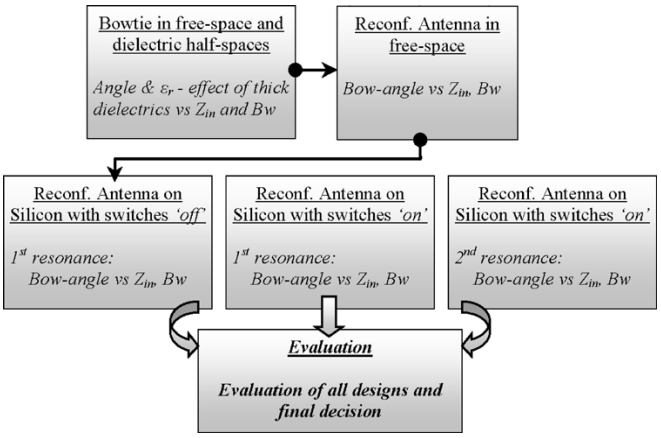

Fig. 7. Schematic of the major steps followed in the optimum antenna design.

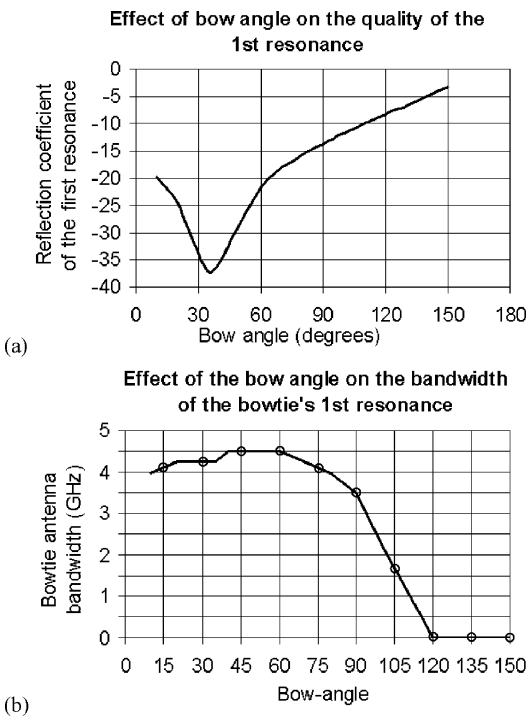

Fig. 8. (a) Quality of matching for different bow angles. (b) Bandwidth of the first resonance as a function of the bow angle for the free-space bowtie antenna.

of $1/\sqrt{\varepsilon_{eff}}$, where $\varepsilon_{eff} = (\varepsilon_r + 1)/2$ is the average of the *Si* and *free-space* permittivities. For a self-complementary antenna fabricated on silicon, the input impedance becomes approximately $Z_{\rm in} = Z_0/\sqrt{\varepsilon_{eff}} = 74.8\ \Omega$. Due to the finite dielectric thickness and antenna size, a deviation from this value is expected and appears in the form of oscillations around it: the real part oscillates between 70 Ω and 120 Ω, while the imaginary part oscillates around $0 \pm j20\ \Omega$. For higher frequencies, input impedance becomes more stable as the structure appears larger. The *Si*-fabricated bowtie antenna's higher resonances repeat every 30 GHz and so its second mode occurs around 48 GHz and does not interfere with the higher Sierpinski mode at 24 GHz. Next, the quality of matching versus the antenna's bow-angle is taken into account and is shown in Fig. 8(a). Bow angles narrower than 90° result in greater oscillations around the constant input impedance value. Finally, the bandwidth of

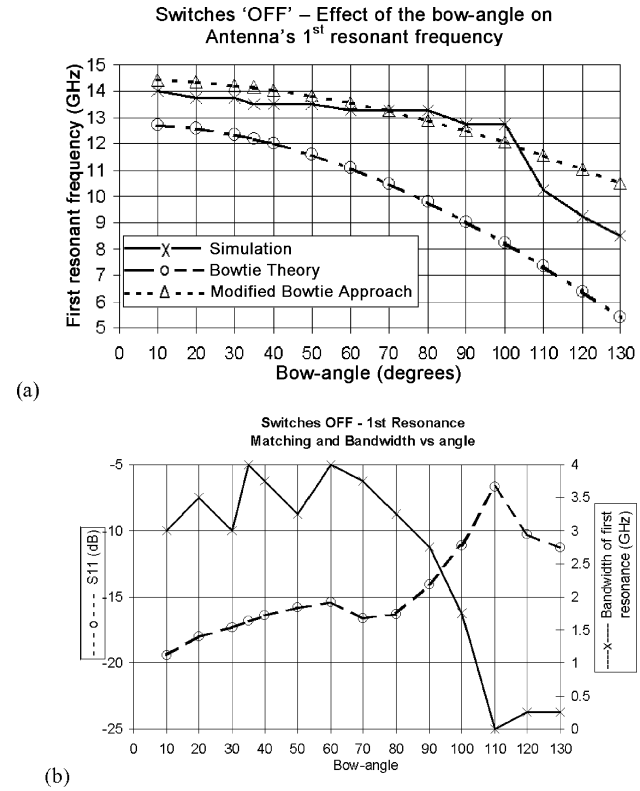

Fig. 9. (a) The first resonance of the antenna as a function of the bow angle for up to 130°. (b) First resonance bandwidth and quality of matching with respect to the bow-angle, for the antenna with switches OFF.

the first resonance with respect to the bow angle is shown in Fig. 8(b). Wider bandwidth is achieved for bow angles smaller than 90° degrees.

B. Sierpinski in Free Space

The Sierpinski gasket antenna in free-space has been analyzed various times in different research works, and thus will not be mentioned here. In [19], some angles of the Sierpinski gasket were tested and results similar to ours were obtained.

C. Sierpinski on Silicon Substrate – All Switches OFF

The free-space studies examined so far serve as an introduction to the more complicated cases with added antenna elements and a considerable thickness of dielectric substrate investigated next. We consider the 1-iteration self-similar antenna fabricated on a *Si* substrate, when all the RF-MEMS switches are OFF. The active region of the antenna for this case is the initial bowtie triangle, while the additional triangles load the antenna in a capacitive manner. Its performance is investigated for different bow angles, and the ones that result in good matching are used in the final evaluation. When the dielectric substrate is thick with high permittivity, like the silicon wafer used here, the antenna's behavior varies from the free-space case studied in section (a). Linearity between the resonant frequency and the cosine of the antenna's half bow angle (as mentioned in [19]), ceases to dominate and also, second resonances may occur with less predictable periodicity. The first resonant frequency with respect to the bow-angle is shown in Fig. 9(a). From the results it can be seen that the resonant frequency diverges more and more for wider bow-angles,

from the predicted one when the antenna is placed on a dielectric half-space. This means that the capacitive coupling is greater and thus it increases the antenna's effective surface for wider angles. It was found that one can account for this nonlinear effect of both capacitive coupling and finite thickness of the substrate, by multiplying the half bow-angle with a number equal to 2/3. This rule-of-thumb yielded good agreement between analytical and simulated results. From then on, this approach will be referred to as the *modified bowtie approach*. Equation (1) gives the first resonant frequency as a function of the antenna's bow-angle, structural dimensions and materials as

$$f_{1_off} = 0.21 \cdot \cos\left(\frac{2}{3} \cdot \frac{\alpha}{2}\right) \cdot \frac{c}{h \cdot \sqrt{\varepsilon_{eff}}} \tag{1}$$

where ε_{eff} is the effective relative permittivity, α is the bow angle, c is the speed of light and h is the height of one antenna's active monopole.

The *modified bowtie approach* results are shown in Fig. 9(a), superimposed with the frequencies given by the *bowtie theory* that considers an infinitely-thick dielectric substrate and does not account for the capacitive coupling, and with the "*simulated*" results that consider both the finite thickness of the substrate and the capacitive coupling between the antenna elements, for comparison purposes. The *modified bowtie approach* was found to be in good agreement with the *simulated* results.

The bandwidth of this first resonance with respect to the bow angle was studied next and is shown in Fig. 9(b), along with the quality of matching to a 50 Ω feedline. Large bandwidth was obtained for angles narrower than 90° degrees, similarly to the case of the bowtie antenna in free-space. The widest bandwidth (4 GHz) occurred for bow angles of 35° and 60°. It is useful to note that the difference between this bandwidth and the one (6 GHz) of the initial antenna as shown in Fig. 5(a), is due to the introduction of the feed transition that was not used in the latter case. This bandwidth reduction can be considered as the least important tradeoff. Regarding the matching, any angle below 90° showed a return loss (S_{11}) less than or equal to -15 dB and thus a relatively good match to the feed.

D. Sierpinski on Silicon Substrate – All Switches ON First Resonance

A similar study was accomplished for the reconfigurable antenna with all switches ON. Since for this configuration, the antenna resonates at two frequencies, each one will be studied separately. The results for the first resonance are shown in Fig. 10. Bowtie theory fails to calculate correctly the frequencies for bow-angles larger than 30°. In (2), the constant 0.21 cannot be scaled directly proportional to the antenna's dimensions. It was found that this scaling factor, for the 1-iteration Sierpinski gasket, yields good results if set to 0.28. However, the factor of 2/3 that accounted previously for the capacitive coupling and the dielectric thickness can be used again and as shown in Fig. 10(a), it gives very good agreement between the theoretical and simulated resonant frequencies. The first resonance as a function of the bow angle can be written as:

$$f_{1_on} = 0.28 \cdot \cos\left(\frac{2}{3} \cdot \frac{\alpha}{2}\right) \cdot \frac{c}{h \cdot \sqrt{\varepsilon_{eff}}} \tag{2}$$

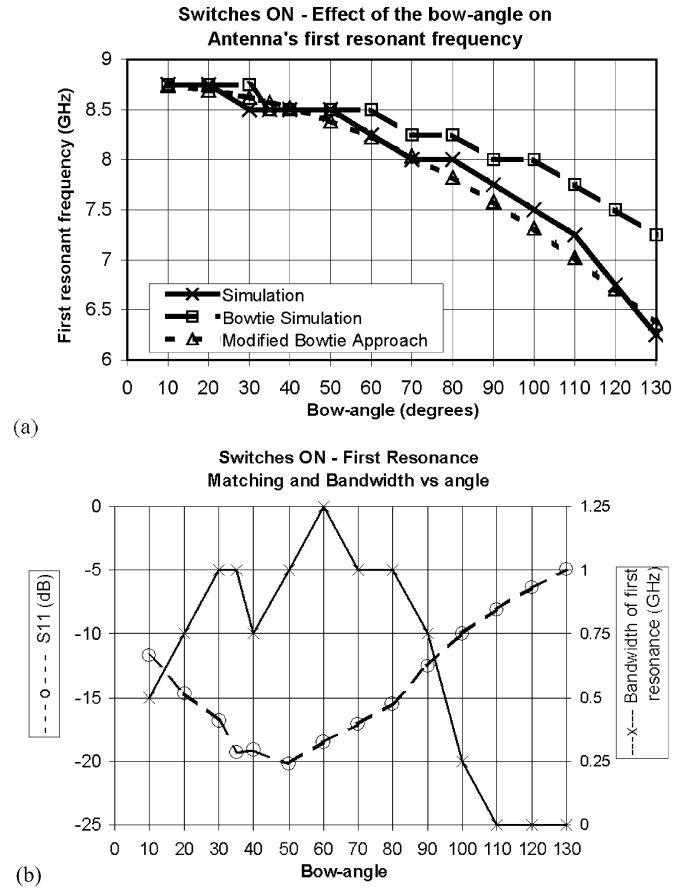

Fig. 10. (a) Effect of the bow angle on the antenna's first resonant frequency when the switches areON. (b) Effect of the bow angle on the matching and the bandwidth of the first resonance.

with the same notation as in (1), but here the height h includes the additional switches and the patches that are connected to them. As the bow angle becomes larger, the self-similar antenna's active area becomes slightly larger and so it resonates at increasingly lower frequencies. This suggests that capacitive coupling between the triangles increases, and additional parts of the structure radiate causing the active area to enlarge. At the same time, the triangular gap in the structure defines different current paths on the antenna, and practically reduces its effective area increasing its resonant frequency. The combination of both phenomena and the finite thickness of the substrate, affect the antenna's performance. The above imply that the two effects may be independent of each other, or they can be decoupled and therefore the 0.28 constant accounts only for the variation in the antenna's effective area due to the formulation of the hole and for the thickness of the substrate, and thus it does not depend on the length of each triangle's side.

To verify the validity of the above, the *modified bowtie approach* results are shown in Fig. 10(a), superimposed with the frequencies given by the *bowtie simulation* that does not account for the capacitive coupling and the triangular gap, for a bowtie antenna of similar dimensions over finite dielectric, and with the simulated results as well. The simulations of a bowtie over finite dielectric show resonances at higher frequencies indicating that the bowtie antenna is smaller than the Sierpinski. The factor of 0.28 is used successfully and is defined at the narrower available bow angle (10°).

Relatively poor, compared to before bandwidth is achieved for this case, with the maximum occurring for 60° (1.25 GHz) followed by 35° and 40°, with 1 GHz. The input impedance is closer to 50 Ω for angles between 20° and 80°, with the best match occurring for 50° with $S_{11} = -20$ dB, followed by 35° with $S_{11} = -19$ dB.

E. Sierpinski on Silicon Substrate – All Switches ON, 2nd Resonance

A similar analysis approach is made for the second resonance with the switches ON. It is expected that bowtie theory will not calculate the correct resonances for the same reasons as mentioned previously. The second resonance of the reconfigurable antenna uses only the initial bowtie as its main radiator but in reality the antenna appears to be even smaller. It resonates at 25 GHz, which is a frequency 2.9 times higher than that of the first resonance with the switches ON (8.5 GHz), and can be related to the 3 times smaller activated metallic surface of the antenna at this second mode. Another approach similar to that of the first resonance is also presented. When the switches are ON, the antenna resonates for a second time at a frequency (25 GHz), which is almost four times higher than the frequency at which a double-sized Sierpinski antenna with switches OFF and with height equal to the entire antenna arm (3772 μm) would resonate (i.e., 6.17 GHz) for the first time. So, the frequency scaling ratio of the two antennas is: $R_f = 6.17\,\text{GHz}/25\,\text{GHz} = 0.246$. This is also very close to the ratio of the actual activated areas of the two antennas at their respective modes. More precisely, the active area of the initial bowtie of the double-sized Sierpinski with switches OFF is four times larger than that of the initial bowtie of the triangle that is activated at the second mode (25 GHz) of the reconfigurable antenna studied here. When this ratio is used to scale the frequency factor of the Sierpinski with switches OFF in (1), the factor becomes: $F = 0.21/0.246 = 0.84$. The factor used here was 0.83 (which results in a ratio $R_2 = 0.21/0.83 = 0.253$), as it approximated better the simulated results. Once again the modified bowtie approach gave very good approximation for the second resonant frequency given by:

$$f_{2_on} = 0.83 \cdot \cos\left(\frac{2}{3} \cdot \frac{\alpha}{2}\right) \cdot \frac{c}{h \cdot \sqrt{\varepsilon_{eff}}}, \tag{3}$$

with the same notation as in (1). The results of the modified bowtie approach are in very good agreement with the simulations for angles up to 130°, as shown in Fig. 11(a).

At this point, it can be noted, that since the above equations are valid for any antenna angle up to 130°, frequency spacing between the first and the second resonance of the Sierpinski antenna can be given by subtracting (2) from (3), resulting in:

$$\Delta f = 0.55 \cdot \cos\left(\frac{2}{3} \cdot \frac{\alpha}{2}\right) \cdot \frac{c}{h \cdot \sqrt{\varepsilon_{eff}}}, \tag{4}$$

which can be used in general for similar antennas fabricated on thick dielectrics. For our case, this frequency spacing is translated into approximately $\Delta f = 16$ GHz. In Fig. 11(b), the effect of the bow-angle on the bandwidth of the second resonance is shown. Greater that 2 GHz bandwidth is achieved for bow-angles between 15° and 50°. It is also noticed that best matching

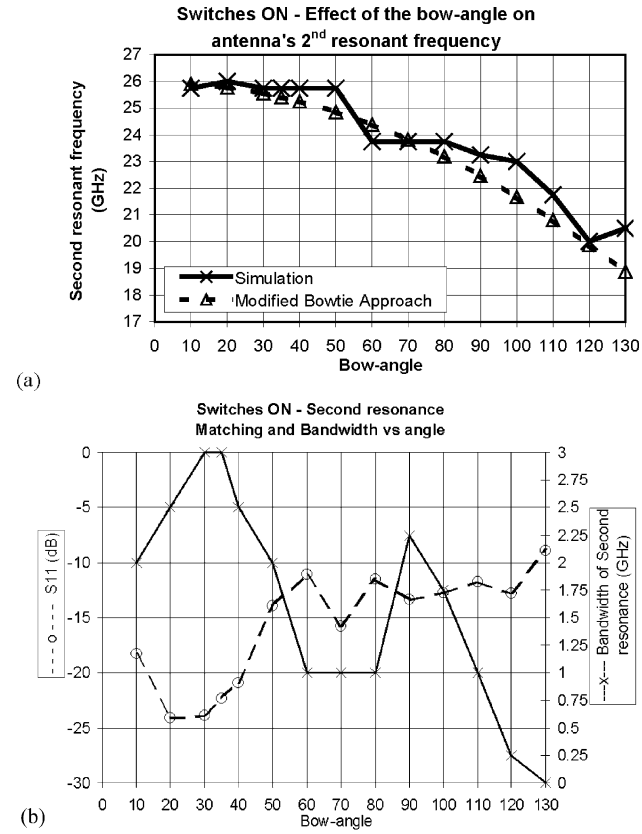

Fig. 11. (a) The second resonant frequency of the reconfigurable antenna as a function of the bow angle for up to 130°, when the switches are ON. (b) Reflection coefficient and bandwidth for the second resonance with different bow angles.

occurs for angles smaller than 50° with S_{11} less than -15 dB, while for larger angles the input impedance results in a return loss between -10 dB and -15 dB.

VI. Final Antenna Design and Measurements

Several antenna designs achieve the desired performance. The criteria used to select the final design are both performance and bandwidth for a particular bow-angle, over the antenna's operational frequencies. Our initial goal was to design a reconfigurable multiband antenna that resonates primarily at 14 GHz, and that can resonate on-demand, at two more frequency bands, preferably around 8 GHz and 24 GHz. Almost all the simulated antennas exhibited radiation patterns similar to that of a planar dipole at their respective resonances, while different applications may require different antenna designs.

Antennas with bow angles less than 100° have, in general, similar to the planar dipole's radiation patterns. For larger angles, the input impedance diverges from 50 Ω and modes with different radiation patterns are being excited. At 8 GHz, antennas with bow-angles between 20° and 80° are suitable for our application. At 14 GHz, it seems that any antenna with a bow-angle from 10° to 90° would suffice as well. For the third resonance at 24 GHz, we would have to look at an antenna with bow-angle between 50° and 80°, but the input impedance for these angles was not acceptable as the return loss was greater than -15 dB. Therefore, antennas between 10° and 50° need to be considered once more, and the 35° one was chosen due to its slightly greater bandwidth char-

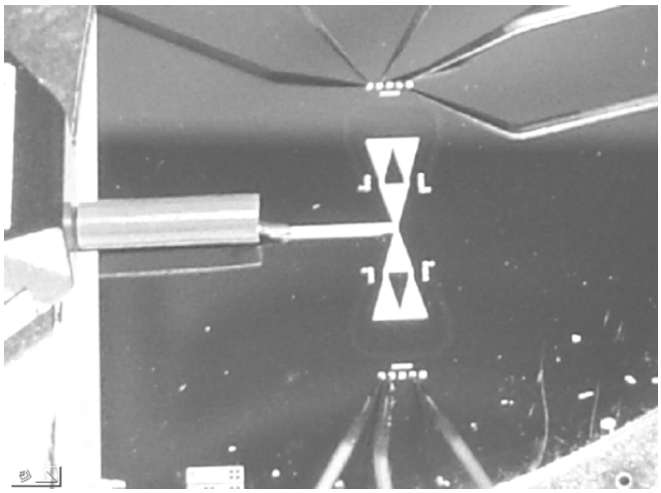

Fig. 12. Photo of the fabricated antenna during measurement.

acteristics. The tradeoff for this choice is a shift at the resonant frequency from 24 GHz to 25.75 GHz, which is not critical at this moment. A photo of the fabricated antenna is shown in Fig. 12.

The dc probe pads consist of 3 grounds and 2 signal lines and have dual pitch (150 and 400) in order to be biased with the available equipment. The pads are placed at the lower and upper ends of the structure. Since they have only 3 ground lines, the third one is used as common ground for two switches, by the use of the antenna's conducting surface. The unpackaged MEMS switches connect and disconnect adjacent antenna triangles. Also, the CPW probe pad connects on the right side of the antenna, only, leaving the left side of the antenna available for future use.

The simulated antenna resonates at three frequencies with a return loss less than -15 dB. These are: $f_{1(\text{sierp 1})} = 8$ GHz, $f_{2(\text{bowtie})} = 13.5$ GHz, and $f_{3(\text{sierp 2})} = 25.75$ GHz with respective bandwidths: $\text{Bw}_1 = 1$ GHz, $\text{Bw}_2 = 4$ GHz and $\text{Bw}_3 = 3$ GHz. Moreover, the bowtie mode is fairly well matched from 17 GHz to 22.5 GHz exhibiting the same radiation pattern as at 14 GHz. This resonance may originate from the feedline, and even though its pattern is also dipole-like, the use of it solely depends on the performance of the measured model. The two nonsymmetric configurations that were mentioned at the beginning of this paper, also exhibited dipole-like simulated radiation patterns.

The entire structure was simulated, fabricated, and measured. The simulated and measured reflection coefficient is shown in Fig. 13. The antenna has three distinct and well-matched resonances, with similar radiation patterns, validating the expected results. It is evident that the antenna's performance changes when the biasing probes are nearby or away from it, due to their large metallic structure that creates reflections of the radiated energy and thus interferes with the antenna's performance. Therefore, when the probes are placed away from the pads, a resonance at 16.5 GHz (with a 14.2 GHz–17.5 GHz bandwidth) is measured. The weak resonance at 21 GHz can also be noticed. Next, when the dc probes come down and touch the biasing pads, but no voltage is applied on them, the antenna resonates at 15 GHz, with a bandwidth from 12.75 GHz up to 17.5 GHz, and covers the desired band at 14 GHz. Since the antenna may constantly be changing configuration, it is energy efficient to keep the probes connected to the pads. Finally, the antenna was measured when

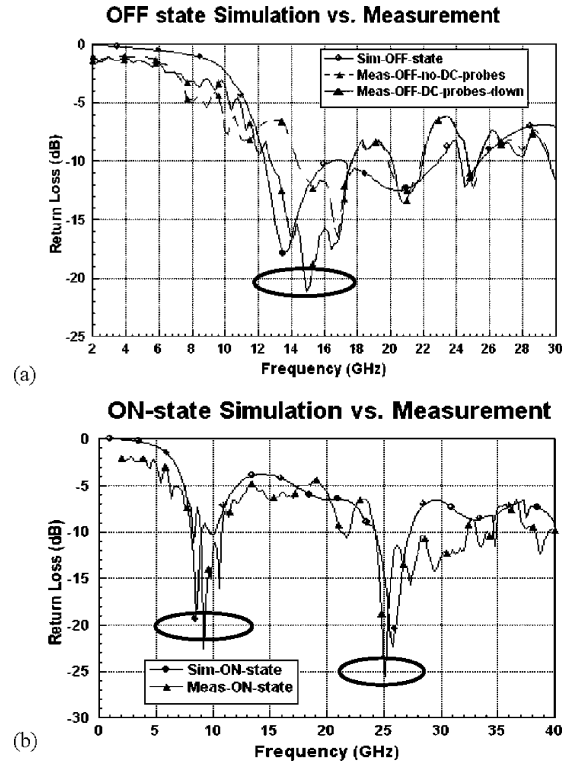

Fig. 13. (a) Return loss of the reconfigurable antenna when all switches are OFF. (b) when all the switches are ON.

all switches are ON. The antenna resonates at two frequencies, very close to the simulated ones. The first one at 9.2 GHz, with a bandwidth of 1.6 GHz, and the second at 25.2 GHz, with a bandwidth from 24.3 GHz up to 28.2 GHz. The antenna maintains a good match up until 32.2 GHz, but it is yet unknown if the radiation pattern maintains its shape. Once again, there is a very weak resonance at 21.5 GHz, which may not necessarily have to be used. The overall measured reflection coefficient showed minor frequency shifts compared to the simulations. The frequency measurements were made using 1 cm thick foam spacers underneath the *Si* wafer, keeping the ground plane as far from the antenna as possible. The spacers' relative permittivity is 1.0001, but it is not thick enough to isolate the ground plane from the antenna completely. Therefore a probable reason for the frequency shifts (especially the 1st resonance at 9.2 GHz) may be addressed on the proximity of the ground plane and on the reflections caused by itself and by the nearby equipment. Still, the measured and simulated results behave similarly and almost coincide at the critical frequencies, which is a very important result considering the detail and size of the actual model.

The antenna's radiation patterns were simulated and measured. In the simulated results, all configurations radiate in the broadside direction, with patterns very similar to each other. The 25.75 GHz simulated pattern is slightly deformed toward the $\varphi = 0°$, most probably due to the long feed structure. Still, tthe antenna's directivity is maximum toward the dielectric side at all frequencies.

The antenna radiation pattern is measured in a unique, far field antenna range that is designed for measuring antennas while they are on an RF probe station. The antenna under test is the transmitting antenna and is fed by a ground-signal-ground RF probe, while the receiving antenna is a half wavelength dipole that is fed by a coaxial cable. The receiving dipole antenna is rotated

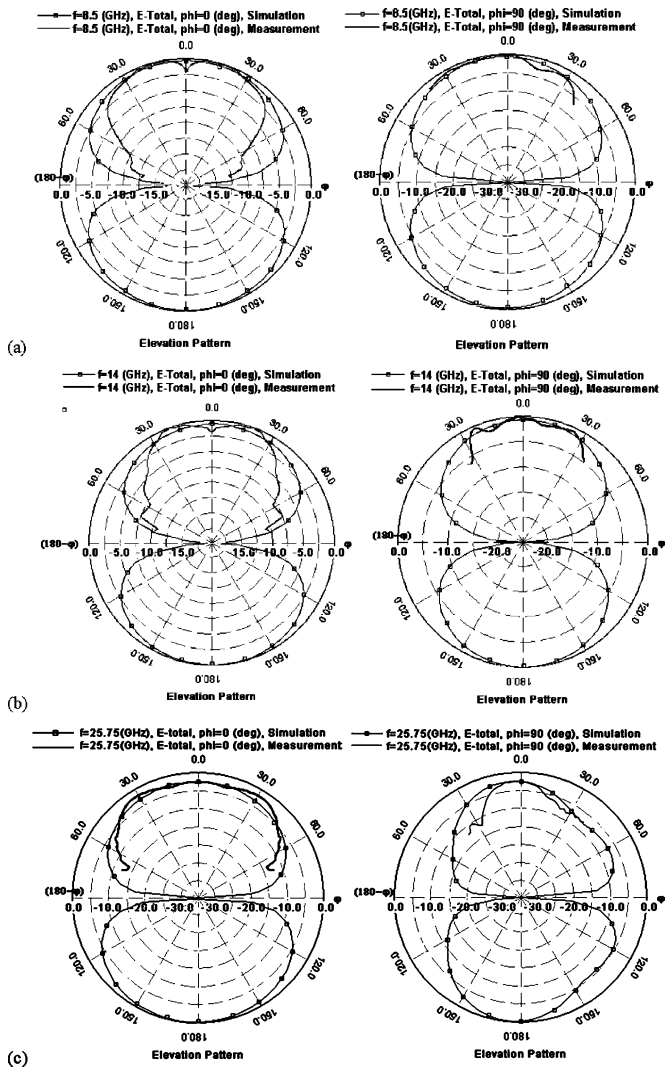

Fig. 14. Measured and simulated normalized radiation patterns at: (a) 8.5 GHz ($\varphi = 0°$ and $\varphi = 90°$), (b) 14 GHz ($\varphi = 0°$ and $\varphi = 90°$), (c) 25.75 GHz ($\varphi = 0°$ and $\varphi = 90°$).

around the antenna under test, with the distance between the two antennas fixed at 9 cm. To bias the MEMS switches, two five-pin dc probes are used, one on each side of the antenna under test. Because the antenna radiates uniformly in the theta direction, the *Si* substrate is placed on 1 cm of absorbing material to minimize effects of the metal wafer chuck. Furthermore, absorbing material is judiciously placed around the antenna under test to minimize the effects of the RF and dc probes, the coaxial dipole and the plexiglass rod that holds it, and the RF probe station. Because the probes and the absorbing material interfere with the measurement system, the data is only plotted over the range where the two antennas are in view of each other. Even with these precautions, there is still ripple in the measured radiation pattern due to the reflecting surfaces. The measured radiation patterns are very close to the simulated ones as shown in Fig. 14. Even though the measurements show some ripple, similarity of all patterns at every resonance is evident as shown from Fig. 15. The reason why some measurements show a small deep in the broadside direction is because there is a thin piece of absorber that had to be added to eliminate radiation from sections of *Au* on the wafer that were causing severe ripple in the patterns, and it partly absorbs

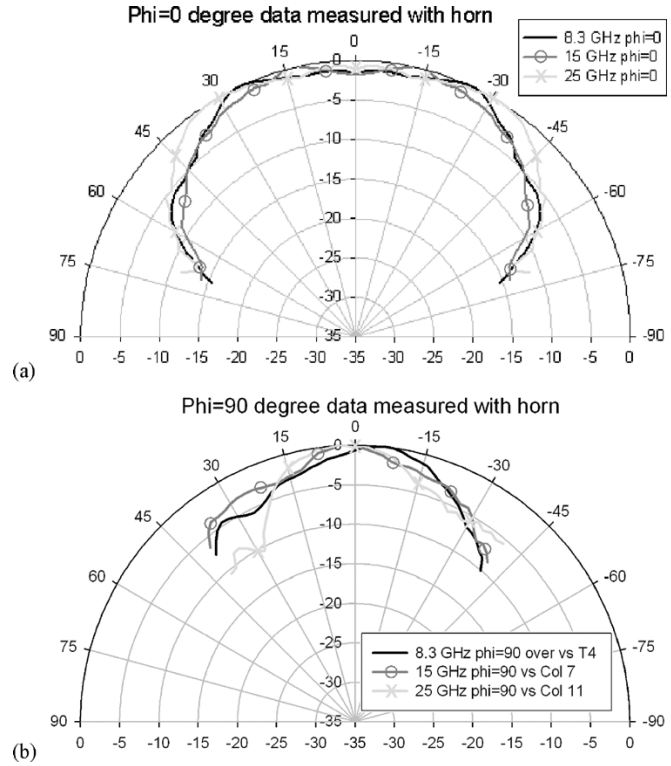

Fig. 15. Comparison of measured radiation patterns at different frequencies. (a) $\varphi = 0°$, 8.3 GHz, 15 GHz and 25 GHz, measurement using a horn antenna, (b) $\varphi = 90°$, 8.3 GHz, 15 GHz, and 25 GHz, measurement using a horn antenna.

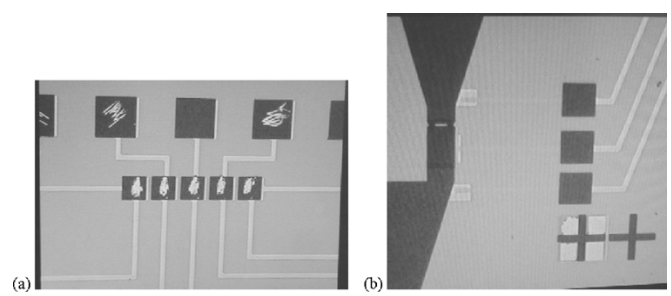

Fig. 16. (a) The dual dc biasing pads on the antenna's upper part, (b) the upper right RF-MEMS switch with its three bias lines. The high-resistive parts of the lines can be seen as the three lines connecting the switch to the dark rectangles.

some of the power at the particular angle. The similarity between measured and simulated results validates the proof of concept of this research.

The antenna was fabricated on a quarter of a silicon wafer with a diameter of 4-inches. Photos showing details of the structure parts with the integrated MEMS switches and the dc pads are shown in Fig. 16. Due to its small size, many antennas can be developed on a single silicon wafer with the same MEMS process, making it suitable for mass-production military or commercial applications.

VII. Summary and Conclusion

A reconfigurable multiple-frequency fractal antenna was designed, fabricated and tested. The antenna radiates in three frequency bands with similar radiation patterns. This system is, to the best of our knowledge, the first functional fully integrated

RF-MEMS reconfigurable fractal antenna ever to be reported. The complete system was simulated and measured and the obtained results were presented in this paper.

Several important things have been learnt during the design, fabrication and measurement of this reconfigurable self-similar antenna. First, the designed antenna needs to be well-matched at all frequencies of interest, for all switch states. This is very important to obtain high reconfigurability and because the connection/disconnection of a switch may lead to mismatched systems.

Also, the integration of the switches to the antenna imposes restrictions on the system design. The antenna structure should be compatible with the switch structure and made with specific materials. The dimensions of the switches often cannot be altered and thus put a low-bound in the size of the antenna system and a high-bound in the power the system can handle.

Next, the effect of the feed transition should be taken into account, as it may degrade the antenna's performance if it's not carefully designed, especially when long feedlines are used.

The need for high-resistive lines to bias the switches is inevitable as metallic lines radiate and deteriorate the antenna's performance. High-resistive lines gave excellent result and did not affect the antenna's impedance or patterns. Their length and resistivity should be carefully chosen in order to not totally isolate the dc probes from the antenna.

From the self-similar antennas studied in this work, a new approach toward their analytical design was developed. The nonlinear effects of the finite dielectric thickness, of the capacitive coupling between the antenna's triangles and of the triangular "gap" in each antenna's arm were taken into account by a "rule of thumb" (the multiplication of the half bow-angle by 2/3) and a constant that accounts for the active area of the antenna (which may be different from its physical area) for each switch state. The presented equations are valid for all antenna angles up to 130 degrees.

Finally, radiation pattern measurements of this antenna cannot be accomplished in a conventional anechoic chamber, as the switches need to be biased during the measurement. In this work, the RF-probe station was transformed into a custom-made anechoic chamber to obtain the measured radiation patterns presented herein.

REFERENCES

[1] E. R. Brown, "RF-MEMS switches for reconfigurable integrated circuits," *IEEE Trans. Microwave Theory and Techniques*, vol. 46, no. 11, pp. 1868–1880, Nov. 1998.

[2] J.-C. Chiao, Y. Fu, I. M. Chio, M. DeLisio, and L.-Y. Lin, "MEMS reconfigurable Vee antenna," in *Proc. IEEE MTT-S Int. Microwave Symp. Dig.*, vol. 4, Jun. 13–19, 1999, pp. 1515–1518.

[3] W. H. Weedon, W. J. Payne, and G. M. Rebeiz, "MEMS-switched reconfigurable antennas," in *Proc. Antennas and Propagation Society Int. Symp.*, vol. 3, Jul. 8–13, 2001, pp. 654–657.

[4] E. R. Brown, "On the gain of a reconfigurable-aperture antenna," *IEEE Trans. Antennas Propag.*, vol. 49, no. 10, pp. 1357–1362, Oct. 2001.

[5] J. Kiriazi, H. Ghali, H. Ragaie, and H. Haddara, "Reconfigurable dual-band dipole antenna on silicon using series MEMS switches," in *Proc. Antennas and Propagation Society Int. Symp.*, vol. 1, Jun. 22–27, 2003, pp. 403–406.

[6] C. Puente, J. Romeu, R. Pous, X. Garcia, and F. Benitez, "Fractal multiband antenna based on the Sierpinski gasket," *Electron. Lett.*, vol. 32, no. 1, pp. 1–2, Jan. 1996.

[7] C. Puente-Baliarda, J. Romeu, R. Pous, and A. Cardama, "On the behavior of the Sierpinski multiband fractal antenna," *IEEE Trans. Antennas Propag.*, vol. 46, no. 4, pp. 517–524, Apr. 1998.

[8] C. T. P. Song, P. S. Hall, H. Ghafouri-Siraz, and D. Wake, "Sierpinski monopole antenna with controlled band spacing and input impedance," *Electron. Lett.*, pp. 1036–1037, 1999.

[9] C. T. P. Song, P. S. Hall, H. Ghafouri-Shiraz, and I. Henning, "Shorted fractal Sierpinski monopole antenna," *Electron. Lett.*, vol. 37, no. 16, pp. 1000–1001, Aug. 2001.

[10] S. R. Best, "Operating band comparison of the perturbed Sierpinski and modified Parany gasket antennas," *Antennas and Wireless Propagation Lett.*, vol. 1, no. 1, pp. 35–38, 2002.

[11] J. P. Gianvittorio and Y. Rahmat-Samii, "Design, simulation, fabrication and measurement of a multiband fractal Yagi antenna," in *Proc. IEEE Topical Conf. Wireless Communication Technology* , Oct. 15–17, 2003, pp. 265–266.

[12] D. E. Anagnostou, G. Zheng, L. Feldner, M. T. Chryssomallis, J. C. Lyke, J. Papapolymerou, and C. G. Christodoulou, "Silicon-etched re-configurable self-similar antenna with RF-MEMS switches," in *Proc. Antennas and Propagation Society Symp.*, vol. 2, Jun. 20–25, 2004, pp. 1804–1807.

[13] G. M. Rebeiz, *RF MEMS: Theory, Design and Technology*. New York: Wiley, 2003.

[14] S. G. Mao, C. T. Hwang, R. B. Wu, and C. H. Chen, "Analysis of coplanar waveguide-to-coplanar stripline transitions," *IEEE Trans. Microwave Theory and Techniques*, vol. 48, no. 1, pp. 23–29, Jan. 2000.

[15] D. E. Anagnostou, M. T. Chryssomallis, and C. G. Christodoulou, "Coplanar waveguide to coplanar stripline transition for a reconfigurable multiband antenna fabricated on silicon," Microwave Wireless Components Lett., submitted for publication.

[16] B. C. Wadell, *Transmission-Line Design Handbook*. Norwood, MA: Artech House, 1991, p. 83.

[17] W. Heinrich, "Quasi-TEM description of MMIC coplanar lines including conductor loss effects," *IEEE Trans. Microwave Theory and Techniques*, vol. 41, no. 1, Jan. 1993.

[18] H. G. Booker, *Journal of IEE (London)*, vol. IIIA, no. 4, pp. 620–627, 1946.

[19] C. Puente, M. Navarro, I. Romeu, and R. Pous, "Variations on the fractal Sierpinski antenna flare angle," in *Proc. Antennas and Propagation Society Int. Symp.*, vol. 4, 1998, pp. 2340–2343.

Dimitrios E. Anagnostou (S'98–M'05) was born in Athens, Greece, in November 1975. He received the Diploma (M.Sc. equivalent) in electrical and computer engineering, from Democritus University of Thrace, Greece, in 2000, and the M.Sc. and Ph.D. in Electrical Engineering from the University of New Mexico, Albuquerque, NM, in 2002 and 2005, respectively.

Since August 2005, he has been working as a Postdoctoral Fellow at the RF Laboratory in the School of Electrical and Computer Engineering of the Georgia Institute of Technology, Atlanta, GA. His research has been published in various Journals and Conferences. His current research work involves reconfigurable RF devices, novel antenna designs, RF-MEMS, packaging on organic substrates, neural networks and image processing.

Dr. Anagnostou is serving as a reviewer for the IEEE TRANSACTIONS OF ANTENNAS AND PROPAGATION. He has been awarded with three research and travel grants during the period 2003–2005. He is a member of the Eta Kappa Nu, and of the Technical Chamber of Greece.

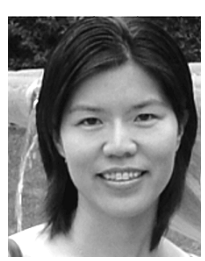

Guizhen Zheng (S'01–M'05) received the B.S.E.E. and M.S.E.E degrees from Tianjin University, China, in 1993 and 1996, respectively, and the Ph.D. degree from the school of Electrical and Computer Engineering of Georgia Institute of Technology, Atlanta, in 2005.

From 1996 to 2000, she worked with Motorola Electronics Ltd. China as an RF design engineer. From 1996 to 1997, she was with Motorola land mobile design center at Penang, Malaysia as an RF engineer. In August 2005, she joined Intel Corporation as a Senior RF packaging engineer. Her current research interest area is in RF/microwave passives design and validation, RF package and interconnects design and validation, RF passives and single-packaged-radio system level performance characterization, RF MEMS switches design, fabrication and integration with the RF front-end-module.

Dr. Zheng is the recipient of the two best paper awards: the 3rd IEEE International Conference on Microwave and Millimeter-Wave Technology (ICMMT 2002), Beijing, China, Aug. 17–19, 2002; and 2004 IEEE Topical Meeting on Si Monolithic IC's in RF Systems, Atlanta, Georgia, Sept. 8 – 10, 2004.

Michael T. Chryssomallis (A'88–SM'00) is received the Diploma in Electrical Engineering and the Ph.D. degree from Democritus University of Thrace, Greece, in 1981 and 1988, respectively.

From 1982 to 1989, he was a Scientific Collaborator; from 1989 to 1994, a Lecturer; from 1994 to 2003, an Assistant Professor; and since 2004, he has been an Associate Professor at Democritus University From Oct. 1997–Jan. 1998, he worked with the Communications Group (director Prof. P. S. Hall) at the University of Birmingham in the areas of active antennas, and with the Wireless Group of the University of New Mexico from April to June 2000, and April to July 2002, in the areas of microstrip antennas and arrays, and smart antennas. He has published several journal and conference papers. His current research interests are in the areas of microstrip antennas, RF-MEMS, smart antennas, and propagation channel characterization.

Dr. Chryssomallis is serving as a Reviewer for the IEEE TRANSACTIONS OF ANTENNAS AND PROPAGATION.

James C. Lyke received the B.S.E.E. degree from the University of Tennessee, Knoxville, the M.S.E.E. degree from the Air Force Institute of Technology, and the Ph.D. E.E. degree through the University of New Mexico.

He has lead over100 inhouse and contract research efforts involving over 50 different multichip module (MCM) designs. His primary pursuits are the development of space microsystems technology through a research group he leads at the Air Force Research Laboratory. He has authored or co-authored over 80 publications, four receiving best paper awards. He has also been awarded six U.S. patents for architecture concepts, and several other patents are in various stages of preparation.

George E. Ponchak (S'82–M'83–SM'97) received the B.E.E. degree from Cleveland State University, Cleveland, OH, in 1983, the M.S.E.E. degree from Case Western Reserve University, Cleveland, in 1987, and the Ph.D. degree in electrical engineering from the University of Michigan, Ann Arbor, in 1997.

He joined the Communication Technology Division, NASA Glenn Research Center, Cleveland, in 1983 where he is now a Senior Research Engineer. During 1997–1998 and 2000–2001, he was a visiting lecturer at Case Western Reserve University. He has authored and coauthored 115 papers in refereed journals and symposia proceedings. His research interests include the development and characterization of microwave and millimeter-wave printed transmission lines and passive circuits, multilayer interconnects, uniplanar circuits, Si and SiC radio frequency integrated circuits, and microwave packaging.

Dr. Ponchak is a senior member of the IEEE Microwave Theory and Techniques Society (MTT-S), a member of the International Microelectronics and Packaging Society (IMAPS), and an Associate Member of the European Microwave Association. He was Editor of a special issue on Si MMICs in the IEEE TRANSACTIONS ON MICROWAVE THEORY AND TECHNIQUES. He founded the IEEE Topical Meeting on Silicon Monolithic Integrated Circuits in RF Systems and served as its Chair in 1998, 2001, and 2006 and was its Digest Editor in 2000 and 2003. He founded the Cleveland MTT-S/AP-S Chapter and serves as its Chair. He has chaired many MTT-S International Microwave Symposium workshops and special sessions. He is a member of the IEEE International Microwave Symposium Technical Program Committee on Transmission Line Elements and served as its Chair in 2003–2005, a member of IEEE MTT-S AdCom Membership Services Committee, and a member of the IEEE MTT-S Technical Committee 12 on Microwave and Millimeter-Wave Packaging and Manufacturing. He received the Best Paper of the ISHM'97 30th International Symposium on Microelectronics Award.

John Papapolymerou (S'90–M'99–SM'04) received the B.S.E.E. degree from the National Technical University of Athens, Athens, Greece, in 1993, and the M.S.E.E. and Ph.D. degrees from the University of Michigan, Ann Arbor, in 1994 and 1999, respectively.

From 1999 to 2001, he was a faculty member with the Department of Electrical and Computer Engineering, University of Arizona, Tucson, and during the summer of 2000 and 2003 he was a visiting professor with The University of Limoges, France. From 2001 to 2005, he was an Assistant Professor with the School of Electrical and Computer Engineering, Georgia Institute of Technology, where he is currently an Associate Professor. His research interests include the implementation of micromachining techniques and MEMS devices in microwave, millimeter-wave and THz circuits, and the development of both passive and active planar circuits on semiconductor (Si/SiGe, GaAs) and organic substrates (LCP, LTCC) for system-on-a-chip (SOC)/ system-on-a-package (SOP) RF front ends. He has authored or coauthored over 120 publications in peer reviewed journals and conferences.

Dr. Papapolymerou received the 2004 Army Research Office (ARO) Young Investigator Award, the 2002 National Science Foundation (NSF) CAREER award, the Best Paper Award at the 3rd IEEE International Conference on Microwave and Millimeter-Wave Technology (ICMMT2002), Beijing, China, and the 1997 Outstanding Graduate Student Instructional Assistant Award presented by the American Society for Engineering Education (ASEE), The University of Michigan Chapter. His student also received the Best Student Paper Award at the 2004 IEEE Topical Meeting on Silicon Monolithic Integrated Circuits in RF Systems, Atlanta, GA. He currently serves as the Vice-Chair for Commission D of the US National Committee of URSI and as an Associate Editor for the IEEE TRANSACTIONS ON ANTENNAS AND PROPAGATION. During 2004, he was the Chair of the IEEE MTT/AP Atlanta Chapter.

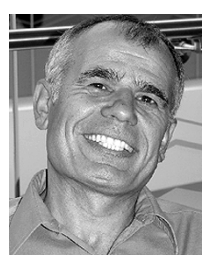

Christos G. Christodoulou (S'80–M'81–SM'90–F'02) received the B.Sc. degree in physics and math from the American University of Cairo, Cairo, Egypt, in 1979, and the M.S. and Ph.D. degrees in electrical engineering from North Carolina State University, Raleigh, in 1981 and 1985, respectively.

He served as a faculty member with the University of Central Florida, Orlando, from 1985 to 1998, where he received numerous teaching and research awards. In 1999, he joined the faculty of the Electrical and Computer Engineering Department, University of New Mexico, Albuquerque, as the Department Chair. He has published more than 200 papers in journals and conferences and authored a book, *Neural Network Applications in Electromagnetics* (Norwood, MA: Artech House, 2001). His research interests are in the areas of modeling of electromagnetic systems, machine learning applications in electromagnetics, smart antennas, and MEMS.

Dr. Christodoulou is a Member of URSI (Commission B). He served as the general Chair of the IEEE Antennas and Propagation Society/URSI 1999 Symposium in Orlando, FL, and as a co-chair of the IEEE 2000 Symposium on Antennas and Propagation for Wireless Communications, in Walham, MA. In 1991, he was selected as the AP/MTT Engineer of the Year (Orlando Section). He is an Associate Editor for the IEEE TRANSACTIONS ON ANTENNAS AND PROPAGATION and the IEEE *Antennas and Propagation Magazine*. He also served as a Guest Editor for a special issue on "Applications of Neural Networks in Electromagnetics" in the *Applied Computational Electromagnetics Society* (ACES) journal.